Published in IET Communications
Received on 6th May 2012
Revised on 13th March 2013
Accepted on 21st March 2013
doi: 10.1049/iet-com.2012.0768

ISSN 1751-8628

# Phase compensation communication technique against time reversal for ultra-wideband channels

*Amir Dezfooliyan, Andrew M. Weiner*

*Department of Electrical and Computer Engineering, Purdue University, West Lafayette, USA*
*E-mail: amir@purdue.edu*

**Abstract:** Phase compensation (PC) prefiltering is experimentally investigated for multipath channels over the frequency band spanning 2–12 GHz, a topic which to the best of the authors knowledge has not been studied in the literature on ultra-wideband (UWB) communications. The authors emphasis is to assess the capabilities of PC compared to time reversal (TR) prefilters over indoor UWB channels regarding multipath suppression, channel hardening, noise sensitivity and high-speed data transmission. Experiments were carried out for PC and TR prefilters in both line-of-sight (LOS) and non-LOS (NLOS) environments. The multipath compression effectiveness is characterised by computing the root-mean-square delay spread and peak-to-average power ratio for actual measured channels and for the IEEE 802.15.4(a) UWB model. The authors study suggests PC outperforms TR considerably in mitigating the multipath channel dispersion. Bit-error-rate (BER) curves have been simulated for data rates in the range of 125–4000 Mbps based on the measured channel responses. The BER simulations suggest that while the TR performance is prohibitively saturated by its residual intersymbol interference for data rates of 500 Mbps and above (especially in NLOS), PC can be used for high-speed data transmissions as fast as 2 Gbps in both LOS and NLOS environments.

## 1 Introduction

Ultra-wideband (UWB) provides several unique advantages like large channel capacity and strong anti-jamming ability for wireless systems [1, 2]. Although UWB has enormous potential for future communication applications, there are a number of challenges, which still are the main topics of current research. In UWB systems, to capture the received energy which is dispersed over a large number of multipath components (MPCs), complex receiver systems (i.e. rake receivers [3, 4]) are necessary. These complex receivers are particularly essential for high data rate communications where intersymbol interference (ISI) degrades the system performance and increases channel bit-error-rates (BERs). A simple transmission scheme called time reversal (TR) can be used [5–7] to reduce receiver's complexity and suppress ISI to some extent. In TR the system impulse response (IR) (which includes IR of the channel, antennas etc.) is flipped in time and used as a pre-matched-filter on the transmitter (Tx) side. TR performance has been studied by several authors for UWB communications [8–16], in most cases with the TR simulated on the basis of measured IRs [8–10] or IEEE UWB channel models [12, 13]. In [8], Monsef *et al.* used TR simulations, based on the IRs measured using a vector network analyser over 600 MHz–6 GHz, to show that although TR has good performance in highly reverberant media, it does not show the same effectiveness in realistic indoor environments. Naqvi *et al.* [14] performed experiments in which they measured BER of TR communications systems for different data rates in the range of 15.6 Mbps–1 Gbps. They carried out experiments both in indoor and in reverberating chamber environments over the frequency range of 0.7–2.7 GHz. They showed BER is dominated by the ISI effects for data rates above 125 Mbps. Simulations have also been used to investigate different schemes that could provide better performance compared to a simple TR system (especially at high data rate) [9, 10, 12, 13]. For instance, in [9, 15], TR is used with the multiple-input–single-output (MISO) structure to obtain a better temporal compression. Oestges *et al.* [10] compared TR performance with that of a minimum mean-squared error (MMSE) prefilter and showed the channel ISI can be suppressed much more strongly by the MMSE prefilter. As they emphasised, the main drawback of MMSE is high implementation complexity which becomes difficult when the number of channel taps increases.

Recently, we utilised a state-of-the-art arbitrary waveform generator to experimentally apply TR over the full frequency range of 2–12 GHz for both biconical omni- and spiral directional antennas [16]. Over this ultra wide frequency range, the temporal resolution of the system, which is inversely proportional to the bandwidth, is extraordinary fine. This provides the capability to resolve most of the MPCs incident at the receiver in a multipath environment which can significantly affect the performance of TR. Based on our measurements, although TR is a powerful technique for compensation of phase distortions associated with broadband frequency-independent antennas, it shows only modest performance in compressing time spread associated with multipath delay.

In the current work, we introduce the phase compensation (PC) prefilter as a solution to suppress ISI in UWB systems and investigate its performance experimentally over the frequency band spanning 2–12 GHz. To the best of our knowledge, this topic has not been reported in the previous literature on UWB communications. PC pre- and post-filters have been extensively used in optical communications and ultrafast optics, for example, [17, 18]. PC has also been previously used [19] to compensate distortion because of spectral phase variations of broadband frequency-independent antennas (e.g. Archimedean spirals) in a situation essentially free of multipath. In the ideal infinite bandwidth case, this is known as All-Pass filtering [20]. For PC the frequency dependent phase of the system response is extracted, and the excitation signals are designed to have the opposite spectral phase. In this way, PC can be seen as an equal gain transmission (EGT) [21] which is implemented in the frequency domain. In equal gain transmitters, which are commonly used in multiple antenna systems, transmitted signals from different antennas are passed through appropriate phase filters to arrive coherently at the receiver. Here, in PC, the spectral phase of the transmit signal cancels the spectral phase distortion of the system response, resulting in a compressed waveform at the receiver.

A special emphasis of our paper is to compare the capabilities of PC and TR prefilters over indoor UWB channels in different regards including multipath suppression, channel hardening, noise sensitivity and impact on high-speed data transmission. We report experiments in which we apply TR and PC prefilters to different measured channel realisations in line-of-sight (LOS) and non-LOS (NLOS) environments. We then calculate temporal compression and peak-to-average power ratio (PAPR) gains of these prefilters and investigate their sensitivity to the noisy channel estimation. To generalise the result beyond our own indoor environment and characterise channel hardening performances, we present simulations based on 1500 channels using IEEE 802.15.4a model. Our studies show that PC has superior performance in compressing UWB multipath dispersions. This point is theoretically proved, independent of any particular channel realisations, in terms of the PAPR gain. In another route to evaluate data transmission performances, BERs are simulated, based on our measured indoor IRs, for received signal-to-noise ratio (SNR) values in the range of −5 to 30 dB. Although TR systems show significant ISI for data rates of 500 Mbps and above (especially in NLOS), PC yields remarkably improved BER which can be used for high-speed transmission of data as fast as 2 Gbps. In general, PC offers potential as a lower complexity (low computation cost because of the efficient fast Fourier transform (FFT) algorithm) alternative for similar prefilters (i.e. optimal MMSE) which have better BER performance compared to TR [22, 23].

The remainder of this paper is organised as follows. In Section 2, we formulate phase-compensation and TR techniques and explore their similarities and differences. We also introduce the parameters we will use to characterise delay spread and temporal compression of PC and TR experiments. Section 3 provides details of the measurement setup, environment layout and research methodology. Examples of the PC and TR measurements, in LOS and NLOS environments, and their performance evaluations based on experimental results and the IEEE 802.15.4(a) (the most comprehensive model for UWB channels) are reported in Section 4. Finally, in Section 5, we conclude.

## 2 Time reversal and PC techniques

### 2.1 Principles of TR and PC

In an ideal case, the received response from TR can be modelled as the autocorrelation of the system IR, which is a symmetric waveform. The waveform transmitted under TR ($X_{\mathrm{TR}}(f)$) and the resulting received response ($Y_{\mathrm{TR}}(f)$) in the frequency domain can be mathematically expressed as

$$X_{\mathrm{TR}}(f) = H^{*}_{\mathrm{Sys}}(f) \tag{1}$$

$$Y_{\mathrm{TR}}(f) = H_{\mathrm{Sys}}(f)X_{\mathrm{TR}}(f) = \left|H_{\mathrm{Sys}}(f)\right|^{2} \tag{2}$$

where $H_{\mathrm{Sys}}$ is the frequency response of the channel, antennas and amplifiers over the measurement bandwidth (up to 12 GHz). Equation (2) shows that in the frequency domain, TR can be seen as a pre-matched-filter, which optimises power allocation over different frequencies in order to maximise the received peak power for a fixed transmitted power. Although TR maximises the power in the central peak, it shows a poor performance in temporal sidelobe suppression [24] which becomes important in high-speed UWB communication regime. Particularly, TR has two principal effects on the frequency domain representation of the received signal (2): (i) compensating the spectral phase distortion; and (ii) squaring the spectral magnitude. The first effect results in concentration of power at the centre of the received response and reduces the root mean square (RMS) delay spread of the channel. The second effect shapes the power spectrum, increasing roll-off in the spectrum (e.g. at high frequencies) and accentuating sharp spectral variations (peaks, fades etc.). Both aspects of the second spectral shaping effect correspond to the aggravation of the overall system amplitude distortion and result in time broadening. Based on whether the PC effect or the spectral shaping effect is stronger, the RMS delay spread of the channel can be either increased or decreased by the TR technique [16].

In UWB channels, because of channel multipath effects, transmitted signals reach the Rx via different paths and attenuations. The result of such random delays and the very large bandwidth is significant frequency selectivity with many sharp fades [25]. In addition, over the UWB range, the frequency dependence of the path loss is significant [26], and channel responses degrade at high-frequency (especially in NLOS scenarios and over long propagation distances). As a result, TR does not show an effective performance in suppression of multipath dispersion, and the received responses from TR have large sidelobes in addition to the main central peak. These sidelobes introduce prohibitively large ISI in high-speed communication channels. Moreover, frequency responses of TR prefilters roll-off at higher frequencies, which results in a poor spectral efficiency [14]. In an effort to achieve a better performance, Naqvi *et al.* [14] introduced a modified TR scheme in which the total UWB bandwidth was divided into $N$ sub-bands. They used ten different passband filters, and normalised the power of each band by using equal power controls. Although they achieved a slightly better BER in their modified TR system, this technique cannot flatten sharp fades of the frequency response and, from a practical point of view, adds complexity.




doi: 10.1049/iet-com.2012.0768

In PC prefilters the channel is excited with the opposite spectral phase of the measured IR to compensate delay distortions of the system. The waveform transmitted under PC ($X_{PC}(f)$) and the resulting received response ($Y_{PC}(f)$) can be mathematically expressed in the frequency domain as

$$X_{PC}(f) = \exp\left(-j \arg\left(H_{Sys}(f)\right)\right) \tag{3}$$

$$Y_{PC}(f) = H_{Sys}(f)X_{PC}(f) = \left|H_{Sys}(f)\right| \tag{4}$$

where $\arg(h_{Sys})$ is the spectral phase of the measured IR of the system. Equation (3) shows the power spectral density of the PC prefilter does not depend on the channel transfer function. Equation (4) indicates PC compensates the spectral phase of the system transfer function, and $Y_{PC}$ is equal to the magnitude of the $H_{Sys}$. Compared to the TR received response (2), PC does not square the spectral magnitude of the channel response (amplitude distortion aggravation), and as a result, intuitively a better temporal sidelobe suppression performance (e.g. temporal PAPR) should be achieved by PC technique. From a theoretical viewpoint, we show in the appendix that the PAPR value for PC always exceeds that for TR (equality only happens when we have a phase-only channel for which PC and TR become formally identical). The PAPR is commonly used as a physical performance indicator in wireless communication systems with pre–post equalisers.

From one point of view, TR and PC can be seen as counterparts to the maximum ratio transmission/combining and EGT/combining techniques [21, 27] which are well known in MISO systems and frequency domain equalisers. From another point of view, PC can be considered as an equaliser that is an intermediate choice between TR and zero forcing (ZF) [22, 25]. In particular, in the frequency domain the received response with PC is the geometric mean of the received responses with TR and ZF, respectively. ZF prefilters, in an ideal case, have a frequency response equal to the inverse of the system transfer function, and are designed to completely compensate channel distortions (zero ISI). In ZF prefilters channel inversion consumes a huge amount of power when the system transfer function exhibits deep fades (when channel transmission is poor). This drawback makes the ZF prefilter costly for a realistic communication system where transmitters are usually limited by some power constraints [25]. In many respects (e.g. maximum received peak power, ISI elimination capability, peak-to-sidelobe ratio), the performance of PC is intermediate between TR and ZF. Although PC does not perfectly eliminate ISI, we experimentally show it can combat the UWB multipath channel dispersions more efficiently compared to TR. Although other prefilters with improved ISI suppression performance compared to TR have been proposed, PC has the potential advantage of lower implementation complexity. The computation cost of this prefilter is low because of the efficient FFT algorithm (with complexity $o(N\log N)$ where $N$ is the number of taps [28]) which is particularly important in UWB systems with large number of taps. However, the complexity is higher than for TR, which requires only flipping the channel IR. As an example of other proposed equalisers [22, 23], Kyritsi *et al.* [22] combined TR and ZF prefilters by using least squares criterion to design a prefilter with acceptable performance over different data rate regimes. Similar to the optimal MMSE prefilter [10] which requires matrix inversion with general complexity of $o(N^3)$ (a comprehensive study on computational complexity of different equalisers are presented in [28]), their prefilter is difficult to implement in a practical UWB system with large delay spread channels corresponding to high number of taps.

### 2.2 Performance characterisation metrics

One of the most useful parameters that characterises the time dispersion introduced by a multipath channel is RMS delay spread ($\sigma$) [25]. The RMS delay value has a direct impact on the ISI of a communication channel [11, 25]. If the symbol time is sufficiently larger than the RMS delay spread (~10 times larger), then the channel is approximately ISI free. To compare the temporal focusing effectiveness of applying TR or PC, we define a temporal compression parameter $C_{rms}$ which shows percentage change of the RMS delay spread after applying the prefilters relative to its initial value

$$C_{rms} = \frac{\sigma_{IR} - \sigma_{TR/PC}}{\sigma_{IR}} \times 100 \tag{5}$$

where $\sigma_{IR}$ and $\sigma_{TR/PC}$ are, respectively, the RMS delay values [25] of the IR, and the corresponding received response from the TR/PC experiment. The parameter $C_{rms}$ provides a measure of the achieved temporal focusing gain by applying the prefilter. We expect this ratio to be as large as possible to have a good compression. Negative values of $C_{rms}$ shows the RMS delay spread of the channel is increased after applying the prefilter. To show the superior performance of PC compared to TR prefilters, we experimentally applied these two techniques over channel realisations at different locations and compared the calculated compression gains. In general, the RMS delay values strongly depend on the selected noise floor level [29]. This threshold level should be as low as possible to capture as much of the real energy as possible, but high enough to avoid the noise effects. In our calculations, we define −42 and −39 dB threshold levels, respectively, for LOS and NLOS measurements and set all components below this level to zero.

In another route to compare the time compression quality of prefilters, we define the PAPR [25] gain ($G_\vartheta$) provided by TR/PC as

$$G_\vartheta = \vartheta_{TR/PC} - \vartheta_{IR} \tag{6}$$

where $\vartheta_{IR}$ and $\vartheta_{TR/PC}$ are, respectively, the PAPR values of the IR and the corresponding received response from the TR/PC experiment. We measure $\vartheta$ over 200 ns time ($T$ = 200 ns) windows for all experiments. The parameter $G_\vartheta$ provides insight about the achieved peak-to-average power gain by implementing TR and PC techniques.

## 3 Experimental system and environment layout

### 3.1 Experimental setup

Fig. 1*a* shows a block diagram of the measurement system. The main components of the transmitter block are an arbitrary waveform generator (Tektronix arbitrary waveform generator (AWG) 7122B), an ultrabroadband amplifier (Picoseconds Pulse Labs 5828A), and the transmitting antenna. The AWG

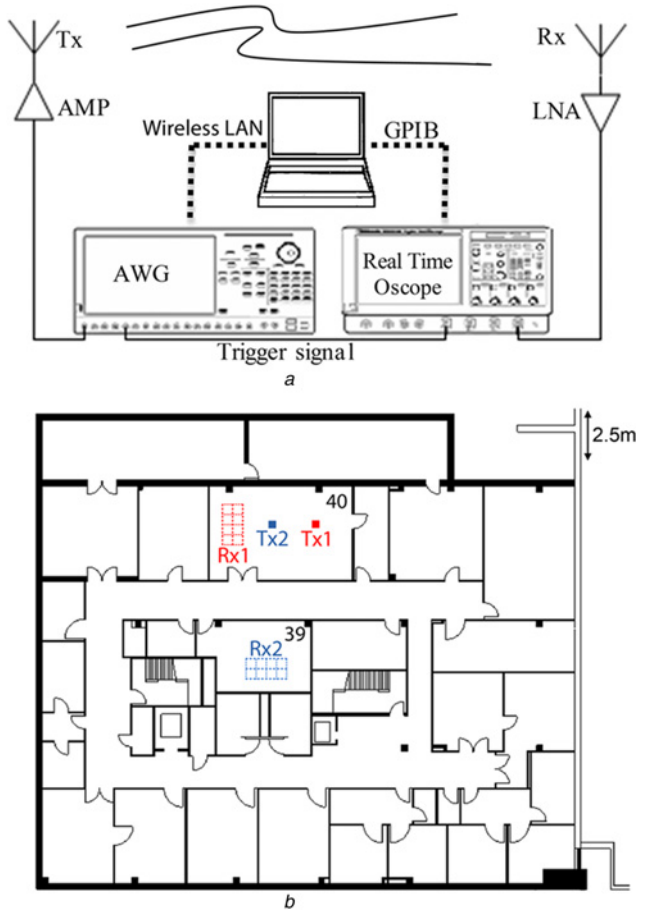


**Fig. 1** *Measurement setup and environment layout*

*a* Block diagram of the measurement setup
*b* Environment layout
Tx1 and Rx1 show, respectively, the positions of the transmitter and the receiver grid for the LOS measurements. Tx2 and Rx2 are the corresponding locations for the NLOS experiments

is used in interleaving mode with an effective RF bandwidth (−6 dB) of 9.6 GHz, maximum sampling rate of 24 GS/s, and maximum peak-to-peak voltage of 0.5 V. Output of AWG is boosted by a 10 dB gain amplifier before transmission through the antenna. In the Rx side, we amplify the received signals using, respectively, 41 and 51 dB amplifier gains in LOS and NLOS measurements. The received signal after amplification is directly connected to a real-time oscilloscope (Digital Serial Analyzer, Tektronix DSA 72004B) with 20 GHz analog bandwidth and maximum real-time sampling rate of 50 GS/s. The oscilloscope is triggered by one of the AWG's digital 'marker' outputs which is synchronised with the transmitted waveform. We used two wideband omni-directional biconical antennas (ELECTRO – METRICS EM-6865, 2–18 GHz) as the transmitter (Tx) and receiver (Rx). Signals recorded by the oscilloscope are stored on a personal computer using general purpose interface bus (GPIB) interface. For NLOS experiments the operator is typically positioned in the same room as the Rx. The AWG is controlled remotely over a wireless local area network which provides a feedback loop to the Tx side. More details about our setup are given in [30].

### 3.2 Environment layout

Experiments have been carried out in the subbasement of the material science and electrical engineering (MSEE) building at Purdue University for which the floor plan is shown in Fig. 1*b*. To observe channel variations, in each LOS and NLOS scenario the Rx antenna is moved along a track to scan a 1.2 m × 2.4 m area, while the Tx antenna is kept at the same location. The minimum inter-element spacing over each grid is 60 cm which corresponds to 15 total measurement points. The LOS experiments (Tx1–Rx1) were conducted in a large laboratory (room 40 in Fig. 1*b*) which contains metallic desks, cabinets, computers and scattering objects of different sizes with average propagation distance of 3.5 m. For NLOS measurements (Tx2–Rx2), we placed the transmitter in the laboratory 40 and the Rx in room 39 across from the laboratory. In this case there are two cement walls and a hallway in the direct path of the Rx–Tx antennas and the average propagation distance is 14 m.

### 3.3 Research methodology

*3.3.1 Experimental measurements:* For each antenna placement, the experimental procedure for TR/PC measurements consists of three steps (i) channel sounding (ii) waveform calculation for TR/PC and communicating this with some predefined accuracy to the Tx side through the wireless local area network (LAN) and (iii) TR/PC waveform transmission and measurement. In this paper, spread spectrum channel sounding is used for IR measurements. This technique not only provides higher dynamic range compared to the pulse excitation method [30], but also has a short acquisition time (compared to the frequency domain channel excitation method which uses vector network analysers) which makes it more suitable for time varying channel measurements. We use an up-chirp signal defined over 0–12 GHz with 85.3 ns time aperture at 24 GS/s sampling rate for channel excitation. To extract system IRs from the received waveforms, a deconvolution method [30] is implemented. First, we record the sounding waveform without wireless transmission (AWG output is connected to the oscilloscope by an RF cable). Then, the received waveform after propagation through the channel and antennas is deconvolved from the sounding waveform [30].

In the next step, the TR/PC waveforms are calculated based on the measured IR, and sent back through the feedback loop (wireless local area network) with 8 bit resolution to the transmitter side. The waveform calculation for TR consists of resampling the obtained IR at 24 GHz and inverting the result in time. For PC, we first used (3) to calculate the PC prefilter in the frequency domain, and then take inverse Fourier transform to construct the time domain PC waveform for generation by AWG. Finally, these signals are transmitted through the channel, and the received waveforms are recorded using the real-time oscilloscope.

*3.3.2 Simulation procedure:* Since our measured channel responses are almost noise free [30], we use simulation to analyse the noise sensitivity of PC and TR. We add white Gaussian noise to the measured channel realisations and calculate these prefilters based on the noisy channel responses. Then, the temporal compression and PAPR gain performances are evaluated as a function of SNR (defined as the average channel response power to the average noise power in dB scale over −170 ns time window) over −5 to 25 dB in steps of 0.5 dB. The final performance curves are finally plotted based on the average results of the 15 NLOS channel realisations.

To assess the performance of TR and PC in high-speed data transmission, we simulate their BER performance. The




doi: 10.1049/iet-com.2012.0768

**Table 1** Average (Avg) and standard deviation (Std) values for omni-directional experiments over 15 LOS and 15 NLOS locations

| Environment | Experiment | RMS delay $\sigma$, ns | | PAPR $\vartheta$, dB | | FWHM, ps | | Temporal compression gain $C_{\text{rms}}$, % | | PAPR gain $G_{\vartheta}$, dB | |
|---|---|---|---|---|---|---|---|---|---|---|---|
| | | Avg | Std | Avg | Std | Avg | Std | Avg | Std | Avg | Std |
| LOS | IR | 14.4 | 0.9 | 29.4 | 1.2 | – | – | – | – | – | – |
| | TR | 15.4 | 1.5 | 30.4 | 0.6 | 121 | 7.2 | −7.2 | 10.3 | 1.05 | 1.0 |
| | PC | 7.0 | 2.1 | 33.79 | 0.2 | 80 | 2.6 | 51.2 | 15.1 | 4.4 | 1.1 |
| NLOS | IR | 19.9 | 1.3 | 19.15 | 1.46 | – | – | – | – | – | – |
| | TR | 16.7 | 1.6 | 26.6 | 0.67 | 202.5 | 17 | 15.8 | 7.8 | 7.46 | 1.2 |
| | PC | 6.2 | 1.4 | 31.3 | 0.24 | 119 | 8.6 | 69.0 | 6.03 | 12.13 | 1.3 |

In the text, we refer to IR metrics by 'IR-Metrics Name'
TR and PC notations are, respectively, used for TR and PC metrics

simulation is based on transmitting $10^7$ random bits using BPSK (binary phase shift keying) modulation over the measured channel realisations. We use TR and PC prefilters for combating the multipath channel dispersion. On the receiver side, we sample the received signal at the peak of PC/TR and make our decision based on the maximum-likelihood criterion [25]. We assume the receiver to be perfectly synchronised with the transmitter. Simulations are performed as a function of the received SNR (defined as the maximum received peak power to the noise power in dB scale) over −5 to 30 dB in steps of 1 dB for data rates ranging 125 Mbps–4 Gbps. The average BER performances are evaluated by averaging the BER of the 15 channel realisations for LOS and 15 channel realisations for NLOS.

We also compare the performance of PC and TR over the IEEE 802.15.4(a) standard, a comprehensive UWB channel model. In these simulations, we have used the statistical parameters presented in Table 1 of [31] for indoor NLOS residential environments.

## 4 Measurement results and analysis

### 4.1 LOS environment

Fig. 2*a* shows the IR of a specific (but typical) LOS omni-directional antenna over 200 ns time window. The received response consists of different MPCs which extend up to −100 ns time window. More details about IR characteristics measured by omni-directional antennas are presented in [16]. To mitigate the multipath effects, we implement TR and PC prefilters. Experimental TR and PC received responses are compared in Figs. 2*b* and *c*. A key point is that as we can clearly see, sidelobes for PC are considerably smaller compared to those for TR.

We repeated LOS IR, TR and PC measurements over a rectangular grid to observe more channel realisations. In Table 1, we summarise average and standard deviation values of the introduced metrics for these measurements under the LOS section. Average full-width half-maximum (FWHM) durations of the PC and TR responses are, respectively, 80 and 121 ps. The larger FWHM duration observed for TR arises because the received signal falls off more rapidly with frequency because of the squaring operation in (2). The average PAPR for TR and PC are increased, respectively, by 1.05 and 4.4 dB compared to the IR-PAPR. For TR, the small PAPR gain ($G_{\vartheta} = 1.05$ dB) indicates TR does not significantly improve the PAPR value. The presence of the dominant LOS component, which is essentially subject to no spectral phase variation, is one of the reasons for this performance [25]. PC-RMS delay is more than two times less than the IR-RMS, while for TR it is increased by 7.2%. The negative temporal compression gain ($C_{\text{rms}} = -7.2\%$) implies single-input–single-output (SISO) TR cannot decrease the RMS delay spread of the channel, which is consistent with the predicted results by simulations in [9]. The broadening effect of SISO-TR (squaring the spectrum magnitude) counteracts and may even exceed the compression effect (spectral PC); overall, TR does not reduce the RMS delay spread of the channel. However, for PC prefiltering spectral PC is the only effect present, and the observed compression gain is significantly larger. In short, PC not only in average reduces RMS delay of the channel to 49% of its original value, but also gives a 4.4 dB PAPR gain.

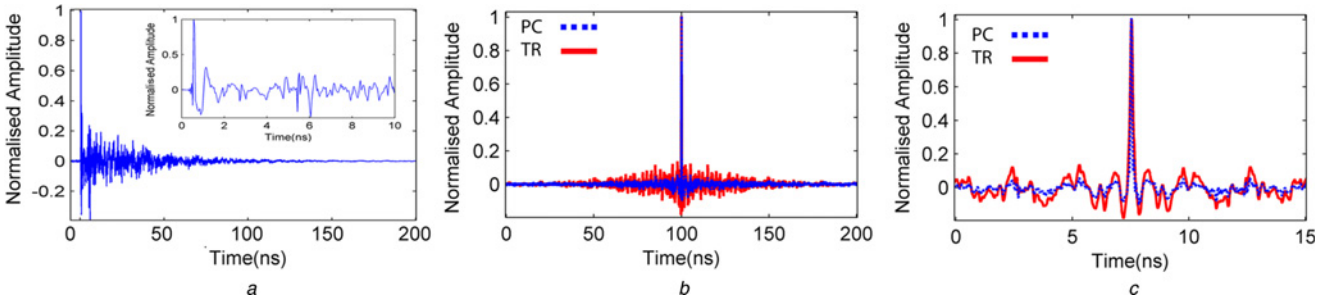


**Fig. 2** *TR versus PC in LOS environments*

*a* IR of LOS omni-directional antennas over 200 ns time window. In the small subfigure, we zoom in on the first 10 ns of the response
*b* Received responses from TR and PC experiments implemented over the channel
*c* We zoom in on the main peak to show details. PC sidelobes are considerably smaller compared to the TR response

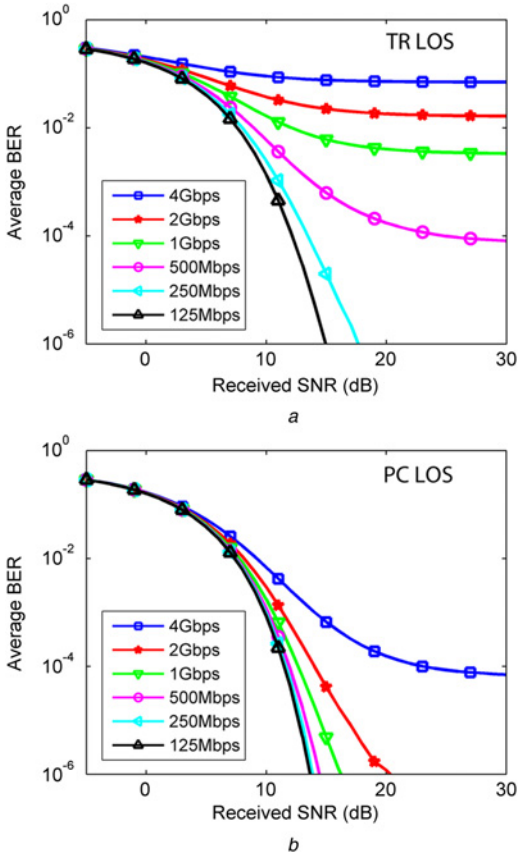


**Fig. 3** *Average BER for LOS PC and TR*

Performance of PC is clearly superior to that of TR in the high data rate regime (500 Mbps and above)
*a* TR
*b* PC

The simulated BER performance averaged over the LOS realisations discussed in Table 1 are presented in Fig. 3. As we can see, for low SNR regime (<5 dB), the system performances are determined by the dominant noise level, and both PC and TR have high BERs. ISI becomes more important for higher SNRs. BER curves for the TR prefilter reach a plateau for data rates of 500 Mbps and above, where increasing the SNR cannot improve the performance any further. In this situation, the system performance is saturated by the ISI originating from TR sidelobes [10]. For the PC prefilter, we have the performance saturation only for the highest (4 Gbps) data rate transmission. This curve levels off at $10^{-4.1}$ BER which is by far better compared to the $10^{-1.1}$ level of the BER plateau of the 4 Gbps TR curve. Although TR and PC curves are close to each other for the low data rate transmission of 125 Mbps, for higher data rates the performance of PC is considerably superior to the TR technique. For instance, the BER for 2 Gbps data rate with PC is below $10^{-4}$ for SNR values larger than 14 dB; however, with TR this curve reaches a floor at $10^{-1.7}$ BER, and better performance cannot be achieved.

### 4.2 NLOS environment

Fig. 4*a* shows an IR of a typical NLOS channel over a 200 ns time window. Unlike Fig. 2*a*, no strong dominant component exists in the channel response. The greater distance and the presence of two cement walls between Tx and Rx lead to an increased number of resolved MPCs and greater high frequency attenuation compared to the LOS scenario discussed earlier. We implement TR and PC prefilters and compare the resulting responses in Figs. 4*b* and *c*. We can clearly see significant superior sidelobe suppression can be achieved using PC prefiltering compared to TR in NLOS UWB channels.

NLOS channel statistics, obtained by moving the receiver over a rectangular grid as described in Section 2, are tabulated in Table 1. This table reconfirms the strength of PC in combating the multipath dispersions. The FWHM of the PC and TR responses are, respectively, 119 and 202.5 ps. These values are larger compared to the corresponding LOS values which is consistent with increased loss for the higher frequencies. The TR and PC performances are improved compared to the LOS scenario. For instance, the PAPR gains are, respectively, −6.4 and −7.7 dB higher for NLOS TR and PC compared to the corresponding LOS values. Absence of the undistorted LOS component is the main reason for this improvement. However, although TR provides PAPR gain, it still gives only modest time compression. The RMS delay of PC is 69% shorter and its PAPR value is 12.13 dB larger than the corresponding NLOS IR values. These values for the TR are only 15.8% and 7.46 dB which again point to superior multipath delay compensation using the PC technique.

To evaluate capabilities of PC against TR beyond our indoor environments, we compare their performance based on 1500 simulated channels using CM2 IEEE 802.15.4a model (NLOS indoor residential environments) [31]. Fig. 5 shows the cumulative distribution function (CDF) of (a) the RMS delay and (b) the PAPR for IR, TR and PC. Both prefilters provide PAPR gain as well as channel hardening, that is, reduction of PAPR variations in terms of 10–90%

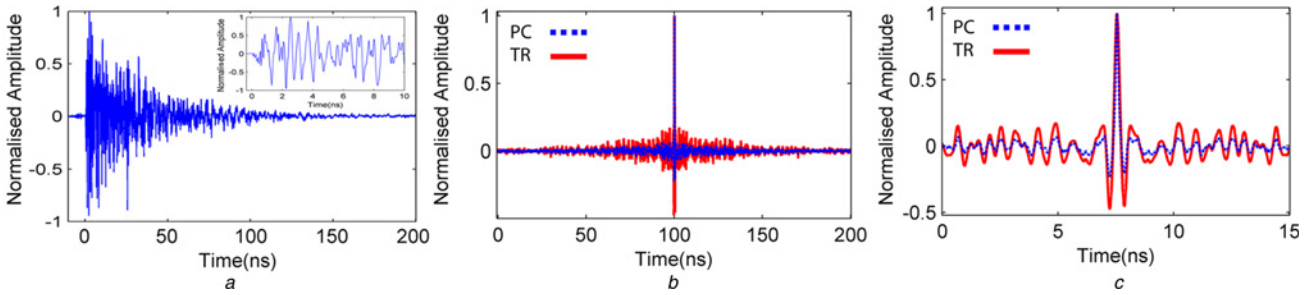


**Fig. 4** *TR versus PC in NLOS environments*

*a* IR of NLOS omni-directional antennas over 200 ns time windows. In the small subfigure, we zoom in on the first 10 ns of the response
*b* Received responses from TR and PC experiments implemented over the channel presented in (Fig. 4*a*)
*c* We zoom in on the main peak to show details. PC sidelobes are considerably smaller compared to the TR response




doi: 10.1049/iet-com.2012.0768

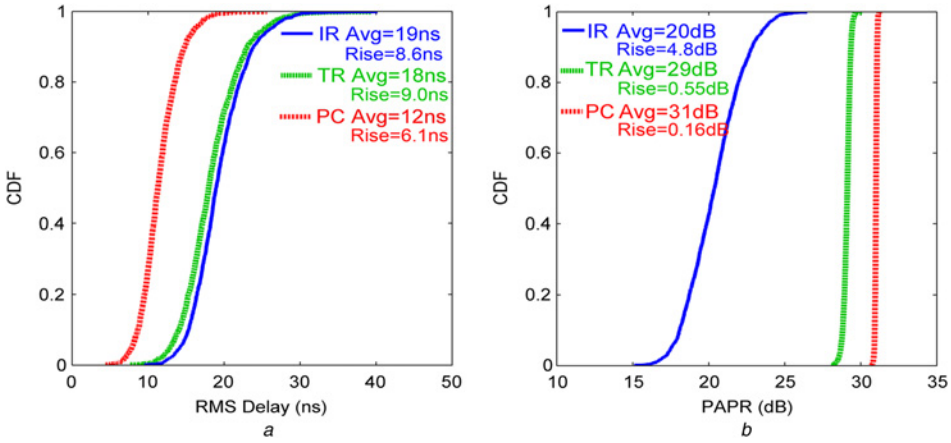


**Fig. 5** *CDF for*

*a* RMS delay
*b* PAPR plotted based on 1500 channel IRs simulated using the IEEE 802.15.4(a) model. On each figure, we show the corresponding average values (Avg) and the 10–90% rise of the CDF (Rise) for IR, TR and PC

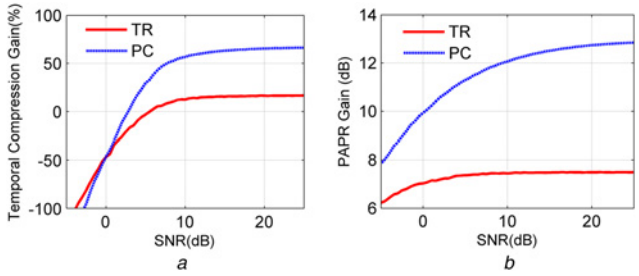


**Fig. 6** *Noise sensitivity for NLOS PC and TR*

*a* Temporal compression gain
*b* PAPR gain

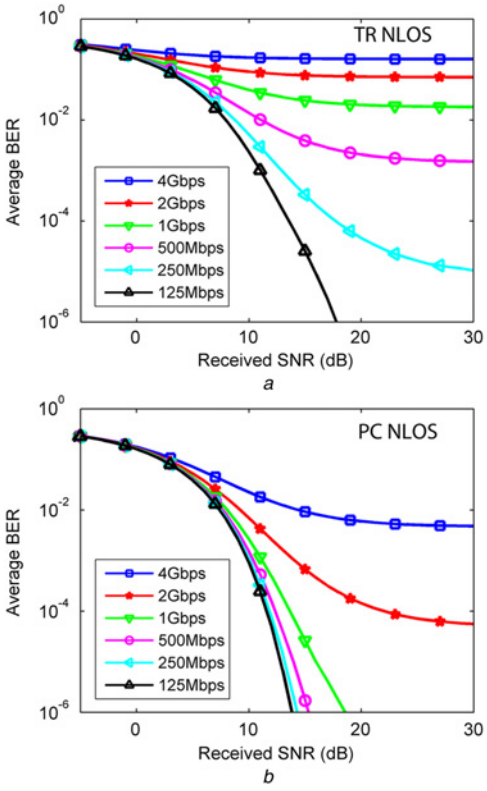


**Fig. 7** *Average BER for NLOS PC and TR*

Performance of PC is clearly superior to that of TR for the data rates of 250 Mbps and above
*a* TR
*b* TC

rise of the CDF. However, PC gives rise to significantly better gain and channel hardening. In terms of RMS delay, PC provides both compression and channel hardening (although much less hardening than is achieved for PAPR). For TR the compression is minimal, and no hardening is apparent. In both cases the simulated temporal compression is smaller than observed experimentally. This difference can be explained by the fact that IEEE 802.15.4a does not take into account important propagation effects like distance dependence, random variation of the path loss exponent and frequency dependence of the path gain [31]. This point shows the importance of experimental implementations.

The sensitivity of prefilter performance to errors in the estimated channel response has been studied for TR in [7]. Using the simulation procedure outlined in Section 3, here we compare the performance of PC and TR prefilters as a function of the SNR in the channel response estimation. Fig. 6*a* shows both prefilters actually increase the RMS delay in low SNR regimes. Temporal compression is achieved for SNRs larger than 2.6 and 5.5 Db, respectively, for PC and TR. The PAPR gain performance is compared in Fig. 6*b*. Although PC is more sensitive to additive noise (its gain drops faster as the SNR decreases), it always provides superior PAPR gain compared to TR.

The simulated BER performance of NLOS PC and TR prefilters, averaged over the channel realisations discussed in the NLOS section of Table 1, are presented in Fig. 7. Comparing Figs. 7 and 3 shows both NLOS PC and NLOS TR responses have inferior BER performances compared to the corresponding LOS scenarios. This can be explained by the fact that NLOS responses have narrower effective bandwidths. This effect is especially important for TR prefiltering for which the frequency rolloff is twice as large in a dB scale (2). As we see in Fig. 7*a*, TR BER curves exhibit error floors for data rates of 250 Mbps and above, for which ISI saturates system performance. For PC in Fig. 7*b*, 2 and 4 Gbps curves level off, respectively, at $10^{-4.25}$ and $10^{-2.3}$ which are considerably better compared to the attained plateau by the corresponding NLOS TR curves

($10^{-1.15}$ for 2 Gbps and $10^{-0.79}$ for 4 Gbps). In general, PC prefilters have substantially superior performance compared to TR. For instance, BER of 1 Gbps PC is below $10^{-4}$ for SNR larger than −13 dB; however, for TR technique, this curve floors at $10^{-1.74}$ and better performance cannot be achieved.

## 5 Conclusion

We investigate PC and TR prefilters in LOS and NLOS environments over the frequency range up to 12 GHz via experiments and simulations. Our work compares the effectiveness of these prefilters in terms of multipath suppression, sensitivity to the noisy estimated responses, channel hardening and data transmission over communication channels. We compare the 'temporal compression' and 'PAPR' gains of these prefilters both based on experimentally measured responses over actual indoor channels as well as simulated channels using IEEE 802.15.4(a). Our study suggests that PC has superior performance in compressing UWB multipath dispersions, a point which is proved theoretically in terms of the PAPR in the appendix. The BERs of the measured channels are presented for different data rates (125 Mbps–4 Gbps) as a function of the received SNR. Our results show PC prefiltering considerably outperforms TR in mitigating ISI because of UWB channel dispersion. Our results suggest that the PC prefilter has the potential to be used in high-speed UWB communication channels as an effective way to combat channel multipath dispersions, provide channel hardening and reduce ISI. In future work, we intend to investigate the spatial focusing performance of PC and TR in different LOS and NLOS environments. Such spatial focusing is critically important for covert communications and multiuser systems.

## 6 Acknowledgments

The authors would like to thank Prof. M.R. Bell and Prof. D.J. Love for their insightful comments and Dr. D.E. Leaird for his helpful technical assistance. This project was supported in part by the Naval Postgraduate School under grant N00244-09-1-0068 under the National Security Science and Engineering Faculty Fellowship program. Any opinion, findings and conclusions or recommendations expressed in this publication are those of the authors and do not necessarily reflect the views of the sponsors.

## 7 References

1 Benedetto, M.G.D., Kaiser, T., Molisch, A.F., Oppermann, I., Politano, C., Porcino, D. (Eds.): 'UWB communication systems – a comprehensive overview' (New York, Hindawi Publishing Corporation, 2006)
2 Yang, L., Giannakis, G.B.: 'Ultra-wideband communications: an idea whose time has come', *IEEE Signal Process. Mag*., 2004, **21**, (6), pp. 26–54
3 Ishiyama, Y., Ohtsuki, T.: 'Performance comparison of UWB-IR using rake receiver in UWB channel models'. Int. Workshop on UWB Systems, May 2004, pp. 226–230
4 Rajeswaran, A., Somayazulu, V.S., Foerster, J.R.: 'Rake performance for a pulse based UWB system in a realistic UWB indoor channel'. IEEE Int. Conf. Communications, ICC'03, Anchorage, AK, USA, 2003, vol. 4, pp. 2879–2883
5 Fink, M., Prada, C., Wu, F., Cassereau, D.: 'Self focusing in inhomogeneous media with time reversal acoustic mirrors'. IEEE Ultrasonics Symp., Montreal, 1989, vol. 1, pp. 681–686
6 Oestges, C., Kim, A.D., Papanicolaou, G., Paulraj, A.J.: 'Characterization of space-time focusing in time-reversed random fields', *IEEE Trans. Antennas Propag*., 2005, **53**, (1), pp. 283–293
7 Tourin, A., Derode, A., Fink, M.: 'Sensitivity to perturbations of a time-reversed acoustic wave in a multiple scattering medium', *Phys. Rev. Lett*., 2001, **87**, (27), pp. 24301-1–24301-4
8 Monsef, F., Cozza, A., Abboud, L.: 'Effectiveness of time-reversal technique for UWB wireless communications in standard indoor environments'. ICECom Conf. Proc., 2010
9 Zhou, C., Guo, N., Qiu, R.C.: 'Experimental results on multiple-input single-output (MISO) time reversal for UWB systems in an office environment'. Proc. MILCOM, Washington DC, 2006
10 Oestges, C., Hansen, J., Emami, S., Kim, A., Papanicolaou, G., Paulraj, A.: 'Time reversal techniques for broadband wireless communication systems'. European Microwave Conf. (Workshop), Amsterdam, The Netherlands, October 2004, pp. 49–66
11 Abbasi-Moghadam, D., Tabataba Vakily, V.: 'Channel characterization of time reversal UWB communication systems', *Springer Ann. Telecommun*., 2010, **65**, (9–10), pp. 601–614
12 Wang, T., Lv, T.: 'Canceling interferences for high data rate time reversal MIMO UWB system: a precoding approach', *EURASIP J. Wirel. Commun. Netw*., 2011, **2011**, pp. 1–10
13 Nguyen, H., Zhao, Z., Zheng, F., Kaiser, T.: 'Preequalizer design for spatial multiplexing SIMO-UWB TR systems', *IEEE Trans. Veh. Technol*., 2010, **59**, (8), pp. 3798–3805
14 Naqvi, I.H., El Zein, G., Lerosey, G., *et al*.: 'Experimental validation of time reversal ultrawide-band communication system for high data rates', *IET Microw. Antennas Propag*., 2010, **4**, pp. 643–650
15 Dezfooliyan, A., Weiner, A.M.: 'Experimental test-bed for studying multiple antenna beamforming over ultra wideband channels up to 12 GHz', *IEEE Wirel. Commun. Lett*., 2012, **1**, pp. 520–523
16 Dezfooliyan, A., Weiner, A.M.: 'Experimental investigation of UWB impulse response and time reversal technique up to 12 GHz: omni-directional and directional antennas', *IEEE Trans. Antennas Propag*., 2012, **60**, pp. 3407–3415
17 Heritage, J.P., Weiner, A.M.: 'Advances in spectral optical code-division multiple-access communications', *IEEE J. Sel. Top. Quantum Electron*., 2007, **13**, (5), pp. 1351–1369
18 Weiner, A.M.: 'Ultrafast Optics' (Wiley, New York, 2009, 1st edn.)
19 McKinney, J.D., Peroulis, D., Weiner, A.M.: 'Dispersion limitations of ultra-wideband wireless links and their compensation via photonically enabled arbitrary waveform generation', *IEEE Trans. Microw. Theory Tech*., 2008, **56**, (3), pp. 710–719
20 Oppenheim, A.V., Schafer, R.W., Buck, J.R.: 'Discrete-time signal processing' (Prentice-Hall, 1999), ch. 5, pp. 280–310
21 Love, D.J., Heath, R.W.: 'Equal gain transmission in multiple-input multiple output wireless systems', *IEEE Trans. Commun*., 2003, **51**, pp. 1102–1110
22 Kyritsi, P., Stoica, P., Papanicolaou, G., Eggers, P., Oprea, A.: 'Time reversal and zero-forcing equalization for fixed wireless access channels'. Record of the 39th Asilomar Conf. Signals, Systems and Computers, 2005, pp. 1297–1301
23 Blomgren, P., Kyritsi, P., Kim, A.D., Papanicolaou, G.: 'Spatial focusing and intersymbol interference in multiple-input/single-output time reversal communication systems', *IEEE J. Ocean. Eng*., 2008, **33**, pp. 341–355
24 Ackroyd, M.H., Ghani, F.: 'Optimum mismatched filters for sidelobe suppression', *IEEE Trans. Aerosp. Electron. Syst*., 1973, **AES-9**, pp. 214–218
25 Goldsmith, A.: 'Wireless communications' (Cambridge University Press, 2005)
26 Tesserault, G., Malhouroux, N., Pajusco, P.: 'Determination of material characteristics for optimizing WLAN radio'. IEEE European Conf. Wireless Technologies, 2007, pp. 225–228
27 Adachi, F., Tomeba, H., Takeda, K.: 'Introduction of frequency-domain signal processing to broadband single-carrier transmissions in a wireless channel', *IEICE Trans. Commun*., 2009, **E92-B**, (9), pp. 2789–2808
28 Martin, R.K., Vanbleu, K., Ming, D., *et al*.: 'Implementation complexity and communication performance tradeoffs in discrete multitone modulation equalizers', *IEEE Trans. Signal Process*., 2006, **54**, (8), pp. 3216–3230
29 Muqaibel, A., Safaai-Jazi, A., Attiya, A., Woerner, B., Riad, S.: 'Pathloss and time dispersion parameters for indoor UWB propagation', *IEEE Trans. Wirel. Commun*., 2006, **5**, (3), pp. 550–559
30 Dezfooliyan, A., Weiner, A.M.: 'Evaluation of time domain propagation measurements of UWB systems using spread spectrum channel sounding', *IEEE Trans. Antennas Propag*., 2012, **60**, pp. 4855–4865
31 Molish, A.F., Cassioli, D., Chia-Chin, C., *et al*.: 'A comprehensive standardized model for ultrawideband propagation channels', *IEEE Trans. Antennas Propag*., 2006, **54**, (11), pp. 3151–3166
32 Hardy, G.H., Littlewood, J.E., Polya, G.: 'Inequalities' (Cambridge University Press, 1934)




doi: 10.1049/iet-com.2012.0768

## 8 Appendix

In this appendix, we show that the temporal PAPR for PC always exceeds that for TR (equality only happens when we have a phase-only channel for which PC and TR become formally identical). The TR and PC prefilters can be mathematically expressed in the frequency domain by (1)–(4) in the main text where the system IR, $h_{\text{Sys}}(t)$, is assumed to be confined to a time aperture of $T$.

We define the peak-to-average energy ratio ($\eta$) parameter as follow

$$\eta_{\text{TR/PC}} = \frac{\left|\text{Max}\left\{y_{\text{TR/PC}}(t)\right\}\right|^2}{(1/2T)\int_{-T}^{T}\left|y_{\text{TR/PC}}(\tau)\right|^2\,\text{d}\tau} \tag{7}$$

Note that the received responses from TR and PC are limited to $2T$ which is twice the aperture of the system response (because of the involved convolution operation). Based on the Parseval's theorem and (2) and (4), we have

$$\begin{aligned}\frac{1}{2T}\int_{-T}^{T}\left|y_{\text{TR}}(\tau)\right|^2\,\text{d}\tau &\overset{\text{Parseval}}{=} \frac{1}{2T}\int_{-\infty}^{\infty}\left|Y_{\text{TR}}(f)\right|^2\,\text{d}f\\ &\overset{(2)}{=}\frac{1}{2T}\int_{-\infty}^{\infty}\left|H_{\text{Sys}}(f)\right|^4\,\text{d}f\end{aligned} \tag{8}$$

$$\begin{aligned}\frac{1}{2T}\int_{-T}^{T}\left|y_{\text{PC}}(\tau)\right|^2\,\text{d}\tau &\overset{\text{Parseval}}{=} \frac{1}{2T}\int_{-\infty}^{\infty}\left|Y_{\text{PC}}(f)\right|^2\,\text{d}f\\ &\overset{(4)}{=}\frac{1}{2T}\int_{-\infty}^{\infty}\left|H_{\text{Sys}}(f)\right|^2\,\text{d}f\end{aligned} \tag{9}$$

Considering the fact that TR and PC have non-negative real frequency transfer functions (as defined in (2) and (4)), the peaks of the received responses happen at zero time delay where all the frequency components add up coherently to each other. Mathematically

$$\begin{aligned}\left|y_{\text{TR}}(t)\right|^2 &= \left|\int_{-\infty}^{\infty}Y_{\text{TR}}(f)\text{e}^{\text{j}2\pi ft}\,\text{d}f\right|^2\\ &\overset{(2)}{=}\left|\int_{-\infty}^{\infty}\left|H_{\text{Sys}}(f)\right|^2\text{e}^{\text{j}2\pi ft}\,\text{d}f\right|^2\\ &\le\left|\int_{-\infty}^{\infty}\left|H_{\text{Sys}}(f)\right|^2\left|\text{e}^{\text{j}2\pi ft}\right|\,\text{d}f\right|^2\\ &\xrightarrow{|\exp(\text{j}2\pi ft)|\le 1}\left|\text{Max}\left\{y_{\text{TR}}(t)\right\}\right|^2\\ &=\left|y_{\text{TR}}(0)\right|^2=\left|\int_{-\infty}^{\infty}\left|H_{\text{Sys}}(f)\right|^2\,\text{d}f\right|^2\end{aligned} \tag{10}$$

$$\begin{aligned}\left|y_{\text{PC}}(t)\right|^2 &= \left|\int_{-\infty}^{\infty}Y_{\text{PC}}(f)\text{e}^{\text{j}2\pi ft}\,\text{d}f\right|^2\\ &\overset{(4)}{=}\left|\int_{-\infty}^{\infty}\left|H_{\text{Sys}}(f)\right|\text{e}^{\text{j}2\pi ft}\,\text{d}f\right|^2\\ &\le\left|\int_{-\infty}^{\infty}\left|H_{\text{Sys}}(f)\right|\left|\text{e}^{\text{j}2\pi ft}\right|\,\text{d}f\right|^2\\ &\xrightarrow{|\exp(\text{j}2\pi ft)|\le 1}\left|\text{Max}\left\{y_{\text{PC}}(t)\right\}\right|^2\\ &=\left|y_{\text{PC}}(0)\right|^2=\left|\int_{-\infty}^{\infty}\left|H_{\text{Sys}}(f)\right|\,\text{d}f\right|^2\end{aligned} \tag{11}$$

Using (8)–(11), we have the following expressions for the peak-to-average power ratios of TR and PC

$$\eta_{\text{TR}} = \frac{\left|\int_{-\infty}^{\infty}\left|H_{\text{Sys}}(f)\right|^2\,\text{d}f\right|^2}{(1/2T)\int_{-\infty}^{\infty}\left|H_{\text{Sys}}(f)\right|^4\,\text{d}f} \tag{12}$$

$$\eta_{\text{PC}} = \frac{\left|\int_{-\infty}^{\infty}\left|H_{\text{Sys}}(f)\right|\,\text{d}f\right|^2}{(1/2T)\int_{-\infty}^{\infty}\left|H_{\text{Sys}}(f)\right|^2\,\text{d}f} \tag{13}$$

As a result, to show the PAPR of PC always exceeds that of TR we should prove the following inequality holds

$$\begin{aligned}\eta_{\text{TR}}\le\eta_{\text{PC}} \Leftrightarrow &\left|\int_{-\infty}^{\infty}\left|H_{\text{Sys}}(f)\right|^2\,\text{d}f\right|^3\\ &\le\left|\int_{-\infty}^{\infty}\left|H_{\text{Sys}}(f)\right|\,\text{d}f\right|^2\left|\int_{-\infty}^{\infty}\left|H_{\text{Sys}}(f)\right|^4\,\text{d}f\right|\end{aligned} \tag{14}$$

To do this, we use the following theorem which is known as Holder's Inequality [32]:

*Theorem (Holder's inequality):* Let $f(x)$, $g(x)$ $X\rightarrow R$ be two measurable functions, and let $p$, $q\in(0, 1)$ so that $p+q=1$.

Then

$$\left|\int_X f(x)g(x)\,\text{d}x\right| \le \left(\int_X\left|f(x)\right|^{1/p}\,\text{d}x\right)^p\left(\int_X\left|g(x)\right|^{1/q}\,\text{d}x\right)^q$$

An equality holds if and only if $|f(x)|^{1/p}$ and $|g(x)|^{1/q}$ are linearly dependent.

To use Holder's inequality, we write (14) as follow (see (15))

Equation (15) is exactly Holder's inequality in which $p=2/3$, $q=1/3$, $f=|H|^{2/3}$ and $g=|H|^{4/3}$. In this case, $f$ and $g$ become linearly dependent (or the equality holds) only when we have a phase-only channel for which PC and TR become formally identical. As a result, (15) is always correct and the temporal PAPR for PC always exceeds that for TR.

$$\begin{aligned}&\left|\int_{-\infty}^{\infty}\left|H_{\text{Sys}}(f)\right|^2\,\text{d}f\right| \le \left|\int_{-\infty}^{\infty}\left|H_{\text{Sys}}(f)\right|\,\text{d}f\right|^{2/3}\left|\int_{-\infty}^{\infty}\left|H_{\text{Sys}}(f)\right|^4\,\text{d}f\right|^{1/3}\\ \Leftrightarrow &\left|\int_{-\infty}^{\infty}\left|H_{\text{Sys}}(f)\right|^2\,\text{d}f\right| \le \left|\int_{-\infty}^{\infty}\left|\left|H_{\text{Sys}}(f)\right|^{2/3}\right|^{3/2}\,\text{d}f\right|^{2/3}\left|\int_{-\infty}^{\infty}\left|\left|H_{\text{Sys}}(f)\right|^{4/3}\right|^3\,\text{d}f\right|^{1/3}\end{aligned} \tag{15}$$